

ION CHEMISTRY IN PHOTON-DOMINATED REGIONS: EXAMINING THE $[\text{HCO}^+]/[\text{HOC}^+]/[\text{CO}^+]$ CHEMICAL NETWORK

C. SAVAGE AND L. M. ZIURYS

Department of Chemistry, Department of Astronomy, and Steward Observatory, 933 North Cherry Avenue,
 University of Arizona, Tucson, AZ 85721

Received 2004 June 11; accepted 2004 August 3

ABSTRACT

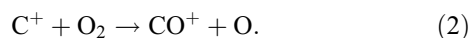
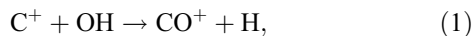
HOC^+ and CO^+ have been detected toward two well-known photon-dominated regions (PDRs), S140 and NGC 2023, using the Arizona Radio Observatory 12 m telescope. The $J = 1 \rightarrow 0$ transition of HOC^+ at 89 GHz and the two spin components of the $N = 2 \rightarrow 1$ line of CO^+ near 236 GHz were observed, as well as the $J = 1 \rightarrow 0$ transitions of H^{13}CO^+ and HC^{18}O^+ . The $J = 3 \rightarrow 2$ line of HOC^+ at 268 GHz was also mapped across the Orion Bar. The $[\text{HCO}^+]/[\text{HOC}^+]$ ratios determined in S140 and NGC 2023 were $\sim 12,408$ and 1913, respectively, values indicative of quiescent molecular gas rather than PDR sources, where the abundance of HOC^+ is thought to be enhanced. However, the beam in both these measurements may contain material from the adjoining molecular cloud, favoring HCO^+ . Alternatively, the $[\text{HCO}^+]/[\text{HOC}^+]$ ratio may vary with A_v in PDR regions. The $[\text{CO}^+]/[\text{HOC}^+]$ ratio in S140 and NGC 2023, at several positions in the Orion Bar, and in other PDRs, on the other hand, falls uniformly in the range ~ 1 –10. In addition, the line profiles of CO^+ and HOC^+ in the Orion Bar look remarkably similar. The syntheses of HOC^+ and CO^+ appear to be correlated in PDRs, most likely through the common precursor, C^+ . The reaction of C^+ and H_2O is thought to preferentially create HOC^+ , as opposed to HCO^+ , and $\text{C}^+ + \text{OH}$ or O_2 leads favorably to CO^+ .

Subject headings: astrochemistry — H II regions — ISM: abundances — ISM: clouds — ISM: molecules — radio lines: ISM

1. INTRODUCTION

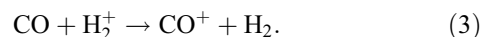
One of the more recent directions in astrochemistry is the study of photon-dominated regions (PDRs). Such regions are formed when high-energy (>13.6 eV) far-ultraviolet radiation from OB stars reaches the edge of a molecular cloud, creating material dominated by photodissociation and photoionization (Sternberg & Dalgarno 1995). This unusually energetic environment is predicted to lead to high abundances of atomic species, including C^+ and Si^+ , as well as unusual molecular ions such as OH^+ , CN^+ , and CS^+ . Molecular and atomic observations have borne out these predictions. For example, measurements of the $158 \mu\text{m}$ fine-structure line of C^+ (e.g., Chokshi et al. 1988; Herrmann et al. 1997) have demonstrated that the abundance of this ion peaks near PDRs. Furthermore, the open-shell ion CO^+ has thus far only been observed toward these regions (e.g., Störzer et al. 1995; Fuente & Martín-Pintado 1997), suggesting that it does not exist in detectable quantities in quiescent molecular clouds.

The CO^+ ion figures prominently in theoretical studies of PDR chemistry (e.g., Tielens & Hollenbach 1985; Sternberg & Dalgarno 1995). In fact, Sternberg & Dalgarno cite the $[\text{HCO}^+]/[\text{CO}^+]$ ratio as a diagnostic of chemical zones within such regions. In particular, CO^+ is prevalent in the C II layer, where most of the carbon is singly ionized. In this model, the C II zone extends from $A_v = 0.7$ to 1.7. Here CO^+ is thought to be primarily formed from singly ionized carbon, namely, by



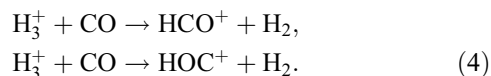
These reactions have rates of about 10^{-9} s^{-1} (Le Teuff et al. 2000; OSU New Standard Model by Herbst), which are typical of interstellar ion-molecule processes. Another pathway

for the formation of CO^+ is through charge exchange from H_2^+ to CO :

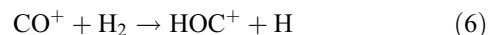
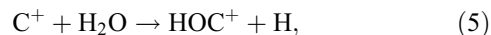


Although this reaction is also fast ($k = 6 \times 10^{-10} \text{ s}^{-1}$), it is not thought to be a major source of CO^+ , because of the scarcity of H_2^+ . Formation of CO^+ from the direct photoionization of CO is not likely either, since its ionization potential is much larger than 13.6 eV. Thus, the reaction of C^+ and OH or O_2 is the dominant source of CO^+ in PDRs.

Another molecule that may serve as a tracer of PDRs is HOC^+ , the metastable isomer of HCO^+ . In molecular clouds, HOC^+ and HCO^+ are predicted to be formed by



The branching ratio of this reaction is somewhat controversial (e.g., DeFrees et al. 1984; Jarrold et al. 1986; Herbst & Woon 1996), but the current consensus is that no more than 10% of HOC^+ is formed. In addition, HOC^+ is rapidly converted to HCO^+ by reacting with H_2 (Smith et al. 2002). These processes lead to an overabundance of HCO^+ in molecular clouds, where the $[\text{HCO}^+]/[\text{HOC}^+]$ ratio is measured to be in the range 2000–6000 (Apponi & Ziurys 1997). In PDRs, however, HOC^+ can also be formed by



(Freeman & McEwan 1987). The branching ratios for these reactions are much more favorable for the production of HOC^+ .

TABLE 1
SUMMARY OF OBSERVATIONS

Source ^a	Species	Transition	ν (MHz)	θ_b (arcsec)	η_c	T_R^* (K)	$\Delta v_{1/2}$ (km s ⁻¹)	V_{LSR} (km s ⁻¹)
S140	H ¹³ CO ⁺	$J = 1 \rightarrow 0^b$	86,754.30	60	0.89	1.18 ± 0.01	2.9 ± 0.9	-7.1 ± 0.9
	HC ¹⁸ O ⁺	$J = 1 \rightarrow 0^b$	85,162.26	60	0.89	0.12 ± 0.01	2.7 ± 0.9	-7.0 ± 0.9
	HOC ⁺	$J = 1 \rightarrow 0^b$	89,487.40	60	0.89	0.005 ± 0.002	5.2 ± 1.7	-7.9 ± 1.7
	CO ⁺	$N = 2 \rightarrow 1^c$						
		$J = 5/2 \rightarrow 3/2$	236,062.55	24	0.45	0.011 ± 0.004	1.2 ± 0.3	-6.0 ± 0.3
NGC 2023	H ¹³ CO ⁺	$J = 1 \rightarrow 0^c$	86,754.30	60	0.89	0.50 ± 0.04	1.4 ± 0.4	10.0 ± 0.4
	HC ¹⁸ O ⁺	$J = 1 \rightarrow 0^c$	85,162.26	60	0.89	0.04 ± 0.01	1.6 ± 0.4	9.6 ± 0.4
	HOC ⁺	$J = 1 \rightarrow 0^c$	89,487.40	60	0.89	0.011 ± 0.003	2.1 ± 0.4	10.3 ± 0.4
	CO ⁺	$N = 2 \rightarrow 1^c$						
		$J = 5/2 \rightarrow 3/2^e$	236,062.55	24	0.45	~0.02 ^e	~1.9 ^e	~12 ^e
Orion Bar	CO ⁺	$J = 3/2 \rightarrow 1/2$	235,789.64	24	0.45	0.013 ± 0.007	1.9 ± 1.0	11.4 ± 1.0
		$N = 2 \rightarrow 1^b$						
		$J = 5/2 \rightarrow 3/2$	236,062.55	24	0.45	0.14 ± 0.02	3.2 ± 0.3	10.4 ± 0.3
NGC 7023	H ¹³ CO ⁺	$J = 1 \rightarrow 0^d$	86,754.30	60	0.89	0.18 ± 0.02	1.0 ± 0.2	2.6 ± 0.2
	HOC ⁺	$J = 1 \rightarrow 0^d$	89,487.40	60	0.89	<0.008
	CO ⁺	$N = 2 \rightarrow 1^b$						
		$J = 5/2 \rightarrow 3/2$	236,062.55	24	0.45	0.016 ± 0.010	1.7 ± 0.6	3.0 ± 0.6

^a Coordinates (B1950.0) of the sources are as follows: S140: $\alpha = 22^h 17^m 42^s$, $\delta = 63^\circ 03' 45''$; NGC 2023: $\alpha = 05^h 39^m 7^s.3$, $\delta = -02^\circ 18' 00''$; Orion Bar: $\alpha = 05^h 32^m 53^s.5$, $\delta = -05^\circ 27' 10''$; NGC 7023: $\alpha = 21^h 00^m 56^s.2$, $\delta = 67^\circ 58' 26''$.

^b Measured with 500 kHz filter banks.

^c Measured with 250 kHz filter banks.

^d Measured with 100 kHz filter banks.

^e Blended with ¹³CH₃OH; see text.

For example, reaction (5) produces 84% HOC⁺, while reaction (6) produces 48%. Given the abundance enhancement of both CO⁺ and C⁺ in PDRs, it is likely that HOC⁺ undergoes preferential formation in these objects as well.

Observational evidence suggests that the abundance of HOC⁺ does undergo significant enhancement in PDRs. Apponi et al. (1999) found the abundance of HOC⁺ relative to HCO⁺ to be significantly larger in the Orion Bar, a well-known PDR, where $[\text{HCO}^+]/[\text{HOC}^+] \sim 270$. However, observations toward M17SW and NGC 2024, two other PDRs, produced ratios of 2260 and 900, respectively, although the ratio in SgrB2(OH) was found to be ~ 360 (Ziurys & Apponi 1995; Apponi et al. 1999). Recently, the abundance of HOC⁺ was also found to be enhanced in Mon R2, a nearby ultracompact H II region, with $[\text{HCO}^+]/[\text{HOC}^+] \sim 460$ (Rizzo et al. 2003), and the lowest ratio thus far of 50–120 has been found in NGC 7023 (Fuente et al. 2003). Curiously, CO⁺ has usually been observed toward objects in which the abundance of HOC⁺ is above average, including the Orion Bar, Mon R2, and NGC 7023 (Störzer et al. 1995; Fuente et al. 2003; Rizzo et al. 2003). Hence, the abundances of CO⁺ and HOC⁺ may be correlated.

Two PDR sources that may serve as additional test cases for this possible correlation are S140 and NGC 2023. S140 is a nearby H II region illuminated by the B0 star HD 211880 (Blair et al. 1978). Optical images, as well as various radio and sub-millimeter maps of the source, show that the PDR is a bright rim on the edge of the molecular cloud (e.g., Minchin et al. 1993, 1995). NGC 2023, in the Orion B molecular cloud complex, is a reflection nebula produced by the B1.5 star HD 37903 (Wyrowski et al. 1997). Although they are prominent PDRs, both sources are smaller and have weaker UV radiation fields than the Orion Bar. For example, the field in S140 is estimated to be $\approx (100\text{--}200)G_0$, while that in NGC 2023 is $\approx 5000G_0$ (Wyrowski et al. 1997); for the Orion Bar, the field is $\approx 4 \times 10^4 G_0$ (Burton et al. 1990). (The quantity G_0 is the Habing field

measured in units of 1.6×10^{-3} ergs cm⁻² s⁻¹ integrated from 912 to 2400 Å; Habing 1968.)

In order to better understand the chemistry of ions in PDRs, we have conducted searches for the $J = 1 \rightarrow 0$ transition of HOC⁺ at 89 GHz and the $N = 2 \rightarrow 1$ lines of CO⁺ near 236 GHz toward S140, NGC 2023, and NGC 7023, using the Arizona Radio Observatory (ARO) 12 m telescope. In addition, we have mapped HOC⁺ $J = 3 \rightarrow 2$ emission across the Orion Bar with an angular resolution of $\sim 24''$. Here we present our results, their analysis, and their implications for chemistry in PDRs.

2. OBSERVATIONS

The data were taken over several observing runs during the period of 1998 December–2004 March using the ARO 12 m radio telescope at Kitt Peak, Arizona.¹ The receivers used were dual-channel, 3 and 1 mm cooled SIS mixers operating in single-sideband mode with typically 20 dB image rejection. The temperature scale (T_R^*) is determined by the chopper wheel method and is corrected for forward spillover losses. The beam efficiencies are estimated to be $\eta_c \sim 0.89$ at $\lambda = 3$ mm and $\eta_c \sim 0.45$ at $\lambda = 1$ mm. The back ends employed were two 256 channel filter banks with different spectral resolutions configured in parallel mode (2×128 channels) for the two receiver channels. For S140, the resolutions used were 100/500 kHz at 3 mm and 250/500 kHz at 1 mm. For NGC 2023, NGC 7023, and the Orion Bar, 100/250 kHz resolutions were used at 3 mm and 250/500 kHz at 1 mm. Data were taken in position-switching mode with the off position 30' west in azimuth, and local oscillator shifts were performed for every measurement.

Single positions were observed toward S140, NGC 2023, and NGC 7023; source coordinates are given in Table 1. Toward

¹ The Kitt Peak 12 m telescope is operated by Arizona Radio Observatory at Steward Observatory, the University of Arizona, with partial support from the Research Corporation.

TABLE 2
OBSERVATIONS OF THE $J = 3 \rightarrow 2$ TRANSITION OF HOC^+
TOWARD THE ORION BAR

Offset ^a (arcsec)	T_R^* (K)	$\Delta v_{1/2}$ (km s^{-1})	V_{LSR} (km s^{-1})
(+40, +20).....	0.04 ± 0.01	1.1 ± 0.6	10.8 ± 0.6
(+20, +10).....	0.06 ± 0.01	2.7 ± 0.6	10.6 ± 0.6
(0, 0).....	0.04 ± 0.01	1.8 ± 0.6	11.3 ± 0.6
(-20, -20).....	0.06 ± 0.01	1.9 ± 0.6	11.1 ± 0.6
(-40, -40).....	0.08 ± 0.01	1.7 ± 0.6	10.3 ± 0.6
(-40, +40).....	0.04 ± 0.01	2.8 ± 0.6	10.0 ± 0.6
(-20, +20).....	0.03 ± 0.01	3.4 ± 0.6	9.9 ± 0.6
(+20, -20).....	0.02 ± 0.01	2.5 ± 0.6	10.8 ± 0.6
(+40, -40).....	<0.02

NOTE.—The frequency is 268,451.50 MHz, and the resolution is 500 kHz.

^a Relative to $\alpha = 05^{\text{h}}32^{\text{m}}53^{\text{s}}.5$, $\delta = -05^{\circ}27'10''$ (B1950.0).

NGC 2023 and S140, the $J = 1 \rightarrow 0$ transitions of H^{13}CO^+ , HC^{18}O^+ , and HOC^+ were observed, as well as the two fine-structure components of the $N = 2 \rightarrow 1$ line of CO^+ . Rest frequencies are listed in Table 1. Only the $J = 1 \rightarrow 0$ lines of H^{13}CO^+ and HOC^+ and one component ($J = 5/2 \rightarrow 3/2$) of CO^+ $N = 2 \rightarrow 1$ were searched for toward NGC 7023. The same CO^+ transition was also observed toward the Orion Bar. In addition, the $J = 3 \rightarrow 2$ transition of HOC^+ was mapped at nine positions across the Orion Bar. The center coordinate and position offsets for the mapping are given in Table 2.

3. RESULTS

The results of these measurements are summarized in Figures 1–7 and in Tables 1 and 2. Both HOC^+ and CO^+ were detected toward S140 and NGC 2023, with line temperatures

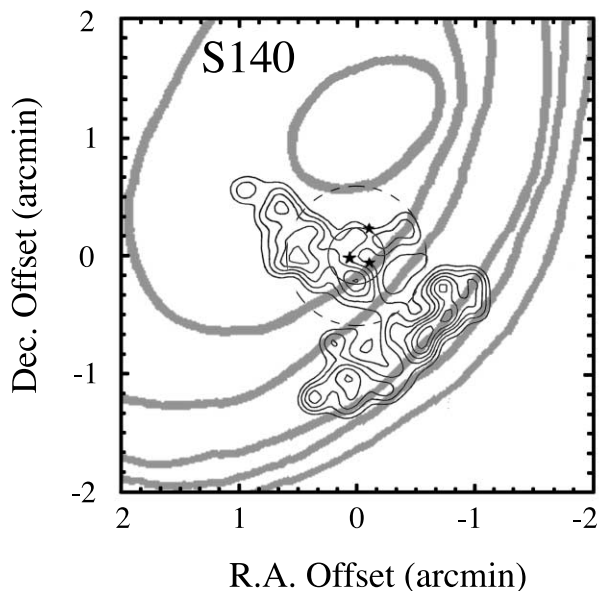


FIG. 1.—S140 PDR and the adjacent molecular cloud, L1204. The ambient cloud is traced by $\text{CO } J = 1 \rightarrow 0$ emission (Blair et al. 1978; *gray contours*), and the PDR is indicated by the black contours, which arise from the $\text{C } I \ ^3P_1 \rightarrow \ ^3P_0$ line (Minchin et al. 1993). The contour levels are 3 K for the CO map and 1 K for the C I emission. The three stars mark the positions of the infrared sources IRS 1, 2, and 3. The position used for the observations is at $\alpha = 22^{\text{h}}17^{\text{m}}42^{\text{s}}$, $\delta = 63^{\circ}03'45''$ (B1950.0), i.e., the (0, 0) position. The dashed circle shows the beam size at 3 mm, while the solid circle represents the 1 mm beam.

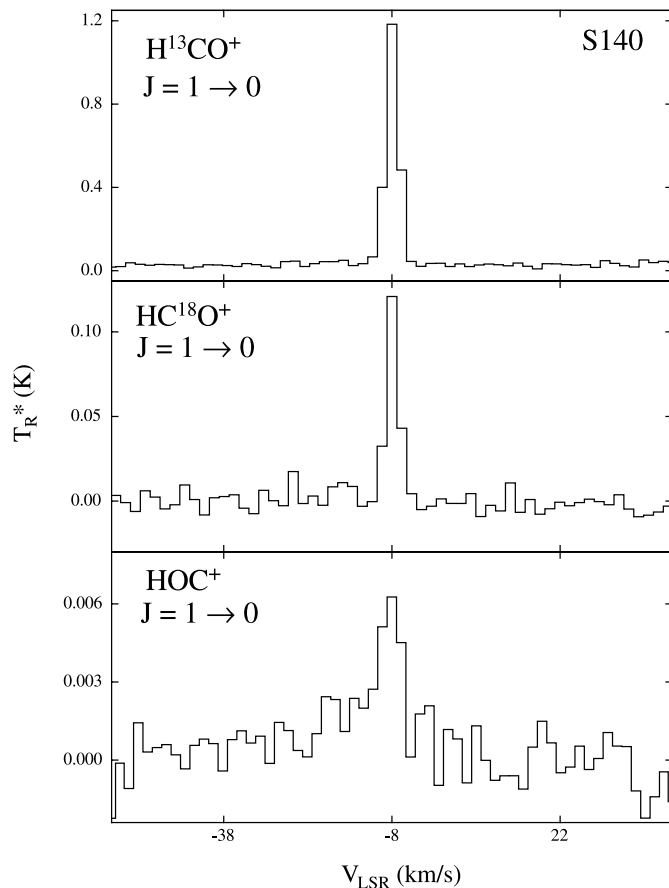


FIG. 2.—Spectra of the $J = 1 \rightarrow 0$ transitions of H^{13}CO^+ , HC^{18}O^+ , and HOC^+ at 86.8, 85.2, and 89.5 GHz, respectively, observed with the ARO 12 m telescope toward S140. Spectral resolution is 500 kHz. The line widths and LSR velocities are similar for all three species, indicating that they arise from the same gas. Integration times per spectrum are 54 minutes, 1 hr, and 43 hr for H^{13}CO^+ , HC^{18}O^+ , and HOC^+ , respectively.

near $T_R^* \leq 10$ mK (see Table 1). However, HOC^+ was not observed in NGC 7023 down to limits of 8 mK, peak to peak. Shortly after these observations were conducted, the detection of HOC^+ toward this object was reported by Fuente et al. (2003). As is discussed below, both sets of measurements are consistent.

3.1. S140

The S140 complex consists of a PDR/H II region on the southwest border of the molecular cloud L1204. The exciting B0 star, HD 211880, is located to the southwest of the bright, ionized $\text{H}\alpha$ rim (Wyrowski et al. 1997). Within the molecular cloud close to the H II region are three embedded infrared sources, IRS 1, 2, and 3, which appear to be associated with outflows (e.g., Wilner & Welch 1994). In Figure 1 a schematic of this source is shown, including the position chosen for these observations ([0, 0] on the figure). The gray contours indicate the position of the molecular cloud, as seen in the $J = 1 \rightarrow 0$ transition of CO (Blair et al. 1978); the solid contours trace the PDR/H II interface region, as observed in the $\text{C } I \ ^3P_1 \rightarrow \ ^3P_0$ line (Minchin et al. 1993). The three stars show the position of the infrared cluster. The 12 m beam is indicated by a dashed contour for the 3 mm observations (HCO^+ and HOC^+) and by a solid contour at 1 mm (CO^+ measurements). The beams at both frequencies encompass a large fraction of the PDR and the molecular cloud, as the figure illustrates.

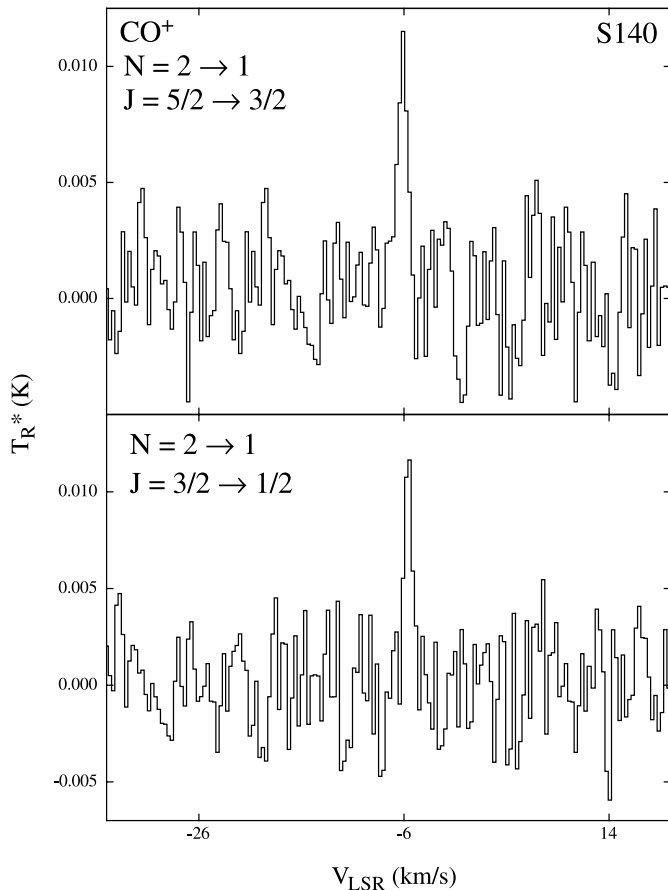


FIG. 3.—Spectra of the two fine-structure components $J = 5/2 \rightarrow 3/2$ and $J = 3/2 \rightarrow 1/2$ of the $N = 2 \rightarrow 1$ transition of CO^+ observed near 236 GHz toward S140 using the ARO 12 m telescope. Spectral resolution is 250 kHz. Both lines are narrow ($\sim 1 \text{ km s}^{-1}$ line widths) and are at the same LSR velocity. The $J = 5/2 \rightarrow 3/2$ line shows no obvious contamination from $^{13}\text{CH}_3\text{OH}$. The spectra were obtained with 66 and 58 hr integration times, respectively.

Figures 2 and 3 display the spectra observed toward S140. In Figure 2 the $J = 1 \rightarrow 0$ transitions of H^{13}CO^+ , HC^{18}O^+ , and HOC^+ are presented using 500 kHz ($\sim 1.7 \text{ km s}^{-1}$) resolution. Spectral lines are present at all three frequencies near LSR velocities of -7 to -8 km s^{-1} , with narrow line widths ($\Delta v_{1/2} \sim 3\text{--}5 \text{ km s}^{-1}$), as expected for this source (e.g., Little et al. 1980). In Figure 3 spectra of the two spin components of the $N = 2 \rightarrow 1$ transition of CO^+ are shown at 250 kHz resolution. The detection of these two features, which have similar velocities and line widths, confirms the presence of this ion in S140. These features have antenna temperatures near $\sim 10 \text{ mK}$, which is substantially less than the previous upper limit in this source of 30 mK for the $J = 5/2 \rightarrow 3/2$ component (Störzer et al. 1995).

Table 1 lists the individual line parameters for each of these spectra. As the table shows, line intensities of CO^+ and HOC^+ are considerably weaker than that of H^{13}CO^+ . In addition, the line widths and LSR velocities are consistent within the errors for the $\text{HCO}^+/\text{HOC}^+$ species. However, for CO^+ the line widths are noticeably narrower ($\Delta v_{1/2} \sim 1$ vs. $\sim 3 \text{ km s}^{-1}$), and the velocities are slightly less negative ($V_{\text{LSR}} \sim -6 \text{ km s}^{-1}$) than the other ions. This effect is likely a consequence of the smaller beam size at 1 mm ($\theta_b \sim 25''$) versus 3 mm ($\theta_b \sim 60''$), which must sample somewhat different gas. In fact, $J = 1 \rightarrow 0$ observations of HCO^+ show that a complex morphology exists for the molecular material near the infrared sources (e.g.,

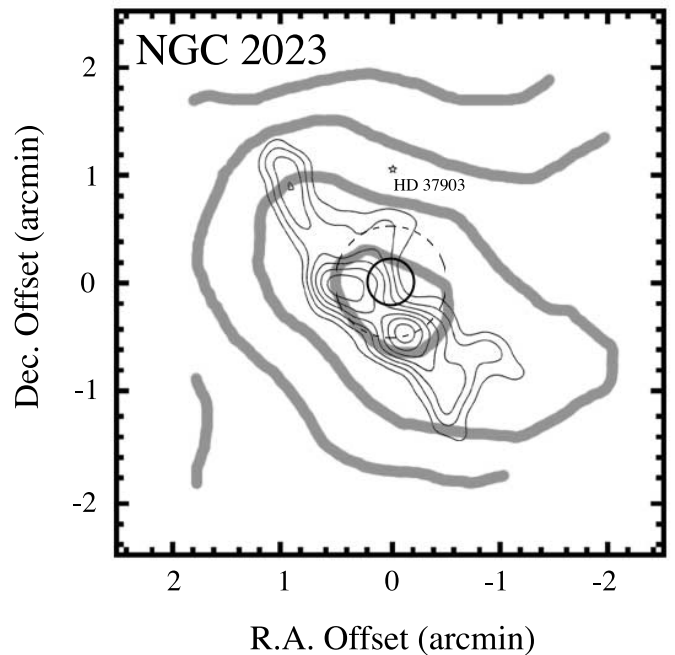


FIG. 4.—PDR/cloud complex of NGC 2023. Emission from the $J = 3 \rightarrow 2$ transition of C^{18}O is indicated by the gray contours, showing the position of the molecular cloud (Wyrowski et al. 1997). The scale is 1.8 K km s^{-1} per contour. The black contours represent emission from $\text{C91}\alpha$ (Wyrowski et al. 2000; scale is $0.8 \text{ mJy beam}^{-1}$), which traces the PDR zone. The location of the exciting star HD 37903 is also indicated. The position observed in this work is $\alpha = 05^{\text{h}}39^{\text{m}}7^{\text{s}}.3$, $\delta = -02^{\circ}18'00''$ (B1950.0) ([0, 0] position), and the beam sizes at 3 mm (dashed circle) and 1 mm (solid circle) are shown.

Wilner & Welch 1994). Variations in LSR velocity and line widths are also seen in CO and C I transitions (Minchin et al. 1993, 1995). Because CO^+ probably samples the PDR gas exclusively and not the ambient molecular cloud, the differences with HCO^+ emission are expected, given the complicated geometry of S140.

Another peculiarity is found in the CO^+ line intensities. The $J = 5/2 \rightarrow 3/2$ component should be roughly 50% more intense than the $J = 3/2 \rightarrow 1/2$ line (Sastry et al. 1981). However, toward S140 they appear to be approximately equal in intensity. This result is most likely a function of signal-to-noise ratio. Within the errors, the line ratio is roughly 2:1. Furthermore, there are no contaminating lines, either in the signal or image sidebands, that could be blended with the $J = 3/2 \rightarrow 1/2$ component. The $K = 2$ components of the $J = 5 \rightarrow 4$ E transition of $^{13}\text{CH}_3\text{OH}$ have been seen to contaminate the $J = 5/2 \rightarrow 3/2$ line in other sources (Fuente & Martín-Pintado 1997), but this would only make the line ratio larger, not smaller. However, as a test we searched for the $K = 0$ component of the same transition of $^{13}\text{CH}_3\text{OH}$ at 235.88117 GHz (Blake et al. 1984). No emission was detected to a noise level of 5 mK, peak to peak.

3.2. NGC 2023

This reflection nebula is associated with the molecular cloud L1630 in the Orion complex (e.g., Lada et al. 1997). The illuminating star, HD 37903, is probably located near the front side of the molecular cloud on the basis of its visual extinction (Wyrowski et al. 1997). As suggested by studies of carbon recombination lines, the PDR is most likely situated near the front of the cloud as well (Wyrowski et al. 2000). This source geometry is illustrated in Figure 4, which shows the $\text{C91}\alpha$

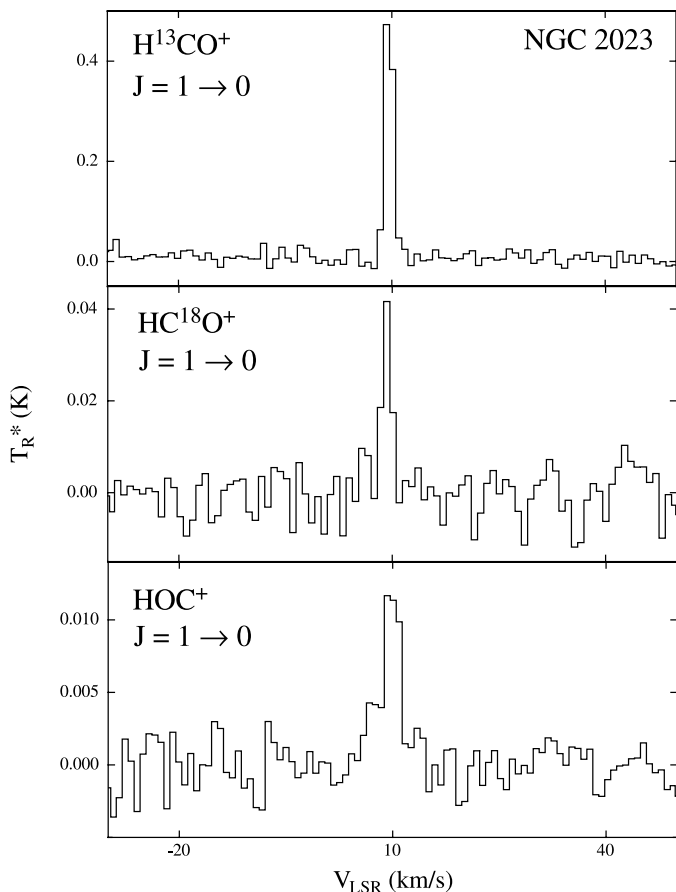


FIG. 5.—Spectra of the $J = 1 \rightarrow 0$ transitions of H^{13}CO^+ , HC^{18}O^+ , and HOC^+ observed toward NGC 2323 using the ARO 12 m telescope. Spectral resolution is 250 kHz ($\sim 1 \text{ km s}^{-1}$). All features appear to be centered near 10 km s^{-1} , as expected for this source. Integration times per spectrum are 1.5, 4.5, and 33 hr for the H^{13}CO^+ , HC^{18}O^+ , and HOC^+ data, respectively.

recombination line emission (*black contours*) from Wyrowski et al. (2000) and that of the $J = 3 \rightarrow 2$ transition of C^{18}O (*gray contours*) from Wyrowski et al. (1997). HD 37903 is indicated by the star. The position used for the observations described here is at (0, 0), and the 3 mm (*dashed circle*) and 1 mm (*solid circle*) beam sizes are shown.

The spectra measured toward NGC 2323 are presented in Figures 5 and 6. Figure 5 displays the $J = 1 \rightarrow 0$ transitions of H^{13}CO^+ , HC^{18}O^+ , and HOC^+ , observed with 250 kHz resolution. All three lines appear at an LSR velocity near 10 km s^{-1} . The HCO^+ features are considerably weaker in this source than in S140 and have narrower line widths ($1.4\text{--}2.0 \text{ km s}^{-1}$). In Figure 6 the CO^+ lines near 236 GHz are presented (250 kHz resolution). In this object, the $J = 5/2 \rightarrow 3/2$ spin component is clearly contaminated by $^{13}\text{CH}_3\text{OH}$, as indicated in Figure 6 (*top*). Here the CO^+ line appears as a shoulder on the methanol feature. The other component of CO^+ (Fig. 6, *bottom*) is uncontaminated, and the intensity ratio between the two components is roughly 2:1. As shown in Table 1, the LSR velocities and line widths are consistent between the HCO^+ , HOC^+ , and CO^+ features. Typical velocities are $V_{\text{LSR}} \sim 10 \text{ km s}^{-1}$, and the line widths are in the range $1.4\text{--}2.1 \text{ km s}^{-1}$, similar to parameters obtained for C91 α , for example (Wyrowski et al. 1997).

3.3. NGC 7023

Observations were also conducted toward NGC 7023, a reflection nebula illuminated by the B3 Ve star HD 200775.

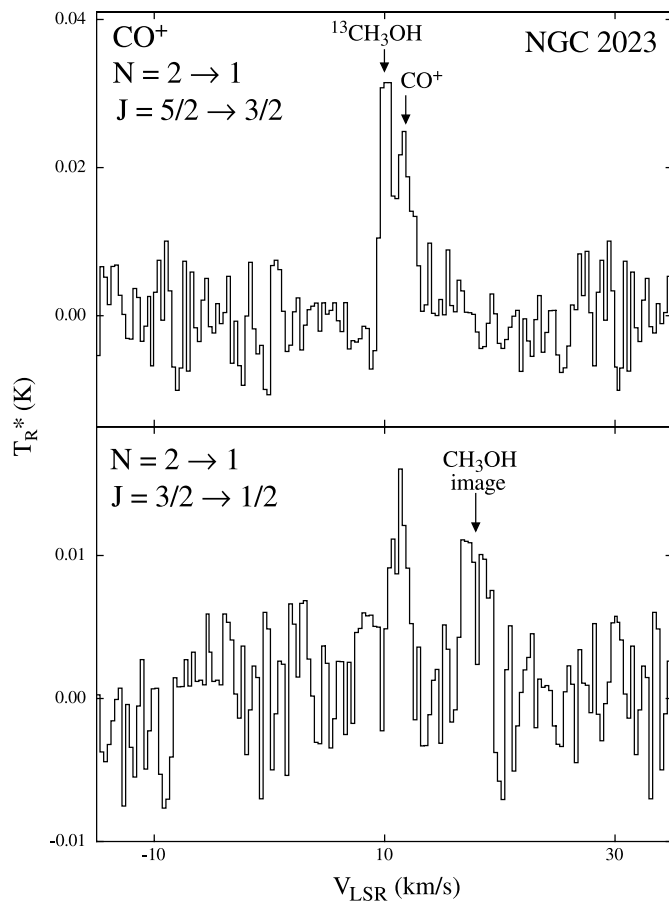


FIG. 6.—Spectra of the two fine-structure components of the $N = 2 \rightarrow 1$ transition of CO^+ observed toward NGC 2323 using the ARO 12 m telescope. The $J = 5/2 \rightarrow 3/2$ line appears as a shoulder on the $K = 2$ asymmetry components of the $J = 5 \rightarrow 4$ transition of $^{13}\text{CH}_3\text{OH}$; they are separated by 1.3 MHz in frequency. The $J = 3/2 \rightarrow 1/2$ line is uncontaminated, hence its smaller line width. The $J = 5/2 \rightarrow 3/2$ and $3/2 \rightarrow 1/2$ spectra were obtained after 12 and 47 hr integration times, respectively.

About $50''$ northwest of the star, which is thought to be in the cavity of a molecular cloud, lies a dense PDR (Fuente et al. 2003). CO^+ had already been detected in this PDR by Fuente & Martín-Pintado (1997); the object seemed an obvious choice to search for HOC^+ emission. This ion, however, was not detected toward the PDR to a limit of 8 mK for T_R^* , peak to peak (or 9 mK for T_R). In fact, the $J = 1 \rightarrow 0$ line of H^{13}CO^+ is also comparatively weak, with $T_R^* \sim 0.18 \text{ K}$ (see Table 1). After these observations were conducted, Fuente et al. (2003) detected the $J = 1 \rightarrow 0$ line of HOC^+ using the IRAM 30 m toward a position just a few arcseconds from the one used here, with an antenna temperature of $T_R \sim 0.02 \text{ K}$. Searches by these authors at other nearby positions for HOC^+ proved negative, suggesting that the emission of this molecule is confined. These authors also searched for the $N = 2 \rightarrow 1$ lines of CO^+ over the same area but found only emission at the same position as HOC^+ . The line intensity of the $J = 5/2 \rightarrow 3/2$ component of CO^+ was $T_R \sim 0.1 \text{ K}$. In contrast, the intensity measured at the 12 m telescope for this transition was $T_R^* \sim 16 \text{ mK}$, or $T_R \sim 35 \text{ mK}$, a factor of 3 lower in intensity. If the same difference in line intensity applies to HOC^+ , then an antenna temperature of $T_R^* \sim 6 \text{ mK}$ is expected for this molecule at the 12 m telescope, slightly below our limit. Consequently, the failure to detect the $J = 1 \rightarrow 0$ line of HOC^+ at the 12 m telescope is likely a result of beam dilution and a

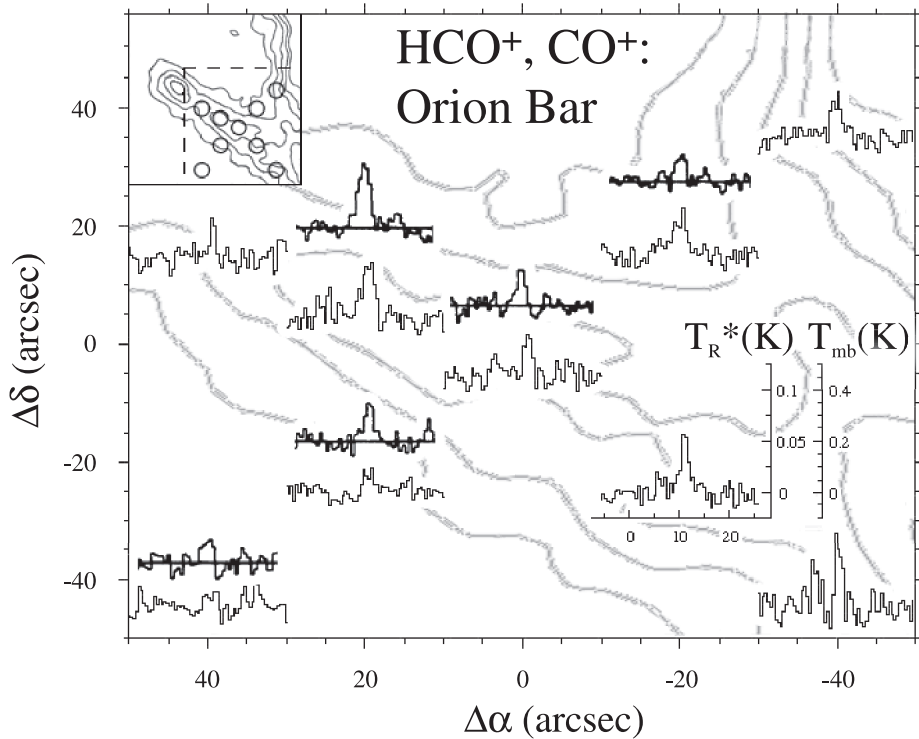


FIG. 7.— $J = 3 \rightarrow 2$ transition of HOC^+ toward the Orion Bar, measured with the ARO 12 m telescope with $\theta_b \sim 24''$. The (0, 0) position is $\alpha = 05^{\text{h}}32^{\text{m}}53^{\text{s}}.5$, $\delta = -05^{\circ}27'10''$ (B1950.0). Overlaid are $N = 2 \rightarrow 1$, $J = 5/2 \rightarrow 3/2$ CO^+ spectra adapted from Störzner et al. (1995), shown with the darker images. The gray contours trace the position of the bar, as seen in $850 \mu\text{m}$ continuum emission (Lis et al. 1998). The insert shows the complete $850 \mu\text{m}$ map and the positions observed in HOC^+ with the 12 m beam size. The T_R^* temperature scale applies to HOC^+ , while the T_{mb} scale is for the CO^+ data. The CO^+ and HOC^+ spectra look quite similar at nearby positions, suggesting a chemical correlation.

clumpy, localized PDR source, as also suggested by Plateau de Bure interferometer maps (e.g., Fuente et al. 1996).

3.4. Orion Bar

The Orion Bar is a well-known PDR source with a high G_0 , and many studies of this object and its chemistry have been conducted by numerous authors (e.g., Tauber et al. 1994; Hogerheijde et al. 1995; van der Werf et al. 1996; Apponi et al. 1999; Fuente et al. 2003). In this study the $J = 3 \rightarrow 2$ line of HOC^+ was measured at nine positions along the bar. As shown in Table 2, which presents line parameters for this transition, the molecule was definitively detected at eight of these positions ($\theta_b \sim 24''$) but not at the (+40, -40) location, which is off the bar itself. A map showing these spectra as a function of position is presented in Figure 7. The spectral line data are superposed over contours of $850 \mu\text{m}$ continuum emission from Lis et al. (1998), which trace the bar region. (An insert shows the complete $850 \mu\text{m}$ map.) Spectra of the $N = 2 \rightarrow 1$, $J = 5/2 \rightarrow 3/2$ transition of CO^+ from Störzner et al. (1995) are also plotted in this figure at positions that coincide with the HOC^+ data; angular resolution here was $\theta_b \sim 15''$. Weak HOC^+ emission is present over most of this region, except at the southeast corner, but the lines are generally stronger along the bar ridge, as traced by higher $850 \mu\text{m}$ contours. This behavior is also followed by CO^+ . Remarkably, the line profiles of both ions look similar, although they were not observed with quite the same beam size.

For additional comparison, the $J = 5/2 \rightarrow 3/2$ component of CO^+ ($N = 2 \rightarrow 1$) was also observed at the (0, 0) position

toward the bar. The parameters of this line are given in Table 1. The line intensities of CO^+ , in terms of T_R , are roughly comparable for the 12 m and 30 m data (Störzner et al. 1995).

4. ANALYSIS

4.1. Column Density Calculations

Column densities of CO^+ , HOC^+ , and HCO^+ in the sources investigated were calculated in the optically thin limit, using the following formula, for $J + 1 \rightarrow J$:

$$N_{\text{tot}} = \frac{3kT_R \Delta v_{1/2} \zeta_{\text{rot}}}{8\pi^3 \nu \mu_0^2 (J+1) [1 - (J_{\text{bg}}/J_{\text{rot}})] \exp(-\Delta E_{\text{gd}}/kT_{\text{rot}})}. \quad (7)$$

Here T_R is the radiation temperature, $\Delta v_{1/2}$ is the FWHM line width, ΔE_{gd} is the energy of the J th level above the ground state, ζ_{rot} is the rotational partition function, ν is the transition frequency, and μ_0 is the permanent dipole moment of the molecule (4.0 D for HCO^+ , 2.8 D for HOC^+ , and 2.8 D for CO^+ ; Haese & Woods 1979; DeFrees et al. 1982; Rosmus & Werner 1982). In the case of CO^+ , which has a $^2\Sigma$ electronic ground state, the column density had to be corrected for the presence of the fine structure. The Rayleigh-Jeans coefficients are $J_T = (h\nu/k)[1/(e^{h\nu/kT} - 1)]$, using a background temperature, T_{bg} , of 2.73 K for J_{bg} and a rotational temperature, T_{rot} , of 15 K for J_{rot} . Because all molecules have large dipole moments, it is reasonable to assume they are subthermally excited ($T_{\text{rot}} < T_{\text{kin}}$). Kinetic temperatures for NGC 2023 have been

TABLE 3
COLUMN DENSITIES AND FRACTIONAL ABUNDANCES

Source	D_{GC} (kpc)	$^{12}C/^{13}C$	$^{16}O/^{18}O$	$N(H_2)$ (cm^{-2})	Species	N_{tot} (cm^{-2}) ^a	f^b
S140	8.2	~69	~517	8×10^{22c}	HCO ⁺	2.3×10^{14}	$\sim 3 \times 10^{-9}$
	8.2	HOC ⁺	5.6×10^{10}	$\sim 7 \times 10^{-13}$
	8.2	CO ⁺	3.1×10^{10}	$\sim 4 \times 10^{-13}$
NGC 2023	8.3	~70	~526	2×10^{22d}	HCO ⁺	4.7×10^{13}	$\sim 2 \times 10^{-9}$
	8.3	HOC ⁺	5.0×10^{10}	$\sim 3 \times 10^{-12}$
	8.3	CO ⁺	6.4×10^{10}	$\sim 3 \times 10^{-12}$
M17SW	5.8	2×10^{23e}	HCO ^{+f}	4.5×10^{14}	$\sim 2 \times 10^{-9}$
	5.8	HOC ^{+f}	2.0×10^{11}	$\sim 1 \times 10^{-12}$
	5.8	CO ^{+g}	1.8×10^{12}	$\sim 9 \times 10^{-12}$
NGC 7023	8.0	~68	~508	3×10^{20h}	HCO ⁺	1.4×10^{13}	$\sim 5 \times 10^{-8}$
	8.0	HOC ⁺	$< 2 \times 10^{10}$	$< 7 \times 10^{-11}$
	8.0	CO ⁺	3.9×10^{10}	$\sim 1 \times 10^{-10}$
Orion Bar	8.3	5×10^{22i}	HCO ^{+f}	8.9×10^{13}	$\sim 2 \times 10^{-9}$
	8.3	HOC ^{+f}	3.3×10^{11}	$\sim 7 \times 10^{-12}$
	8.3	CO ⁺	6.4×10^{11}	$\sim 1 \times 10^{-11}$
Mon R2	8.7	2×10^{21j}	HCO ^{+k}	7.8×10^{13}	$\sim 4 \times 10^{-8}$
	8.7	HOC ^{+k}	1.7×10^{11}	$\sim 9 \times 10^{-11}$
	8.7	CO ^{+k}	5.3×10^{11}	$\sim 3 \times 10^{-10}$

^a Assuming $T_{rot} = 15$ K, unless the value is taken from the literature.

^b Relative to H_2 .

^c Minchin et al. 1993.

^d Wyrowski et al. 1997.

^e Stutzki et al. 1988.

^f Apponi et al. 1999.

^g Störzner et al. 1995.

^h Buss et al. 1994.

ⁱ Hogerheijde et al. 1995.

^j Kutner & Tucker 1975.

^k Rizzo et al. 2003.

estimated to be $T_{kin} \sim 200$ K in regions where C^+ exists (Wyrowski et al. 1997), and Fuente et al. (2003) found $T_{rot} \sim 7$ –31 K from their studies of HOC⁺ in NGC 7023. CO observations toward S140 suggest $T_{kin} \sim 65$ –70 K (Minchin et al. 1993).

The column densities derived for HCO⁺ were calculated from HC¹⁸O⁺ and H¹³CO⁺ and then scaled by the appropriate isotope ratios. The $^{16}O/^{18}O$ ratio was estimated from the following formula, as a function of distance from the Galactic center, D_{GC} :

$$^{16}O/^{18}O = (58.8 \pm 11.8)D_{GC} + (37.1 \pm 82.6). \quad (8)$$

This relationship has been derived from double isotope measurements of H_2CO by Wilson (1999). For $^{12}C/^{13}C$, the carbon isotope ratio gradient, derived also from Wilson (1999), was used:

$$^{12}C/^{13}C = (7.5 \pm 1.9)D_{GC} + (7.6 \pm 12.9). \quad (9)$$

It should be noted that the Galactocentric distances employed in our calculations are slightly different from those in previous publications because of an improved determination of the distance between the Earth and the Galactic bulge (McNamara et al. 2000). The calculated isotope ratios and D_{GC} used for the column density calculations are given in Table 3.

Column densities derived for HOC⁺, CO⁺, and HCO⁺ for NGC 2023, S140, and NGC 7023 are listed in Table 3. (The values given for S140 and NGC 2023 for HCO⁺ are an average based on the ^{18}O and ^{13}C isotopomers.) For comparison, col-

umn densities for M17SW and the Orion Bar are listed as well, taken from Apponi et al. (1999) for HOC⁺ and HCO⁺ and from Störzner et al. (1995) for CO⁺. Also given are the same quantities for Mon R2 (Rizzo et al. 2003).

As shown in Table 3, the HCO⁺ column density of $2.3 \times 10^{14} cm^{-2}$ in S140 is about a factor of 5 higher than in NGC 2023, where $N_{tot}(HCO^+) \approx 4.7 \times 10^{13} cm^{-2}$. However, the column densities of HOC⁺ were similar in both sources, with $N_{tot}(HOC^+) \approx 5.6 \times 10^{10} cm^{-2}$ toward S140 and $5.0 \times 10^{10} cm^{-2}$ toward NGC 2023. The values for CO⁺ are also similar, with $N_{tot}(CO^+) = 3.1 \times 10^{10} cm^{-2}$ toward S140 and $6.4 \times 10^{10} cm^{-2}$ toward NGC 2023. Also given in Table 3 are fractional abundances of the three ions, relative to H_2 . These values were calculated using literature values of H_2 column densities. In S140 $N(H_2) \approx 8 \times 10^{22} cm^{-2}$ (Minchin et al. 1993), in NGC 2023 $N(H_2) \approx 2 \times 10^{22} cm^{-2}$ (Wyrowski et al. 1997), and $N(H_2) \approx 3 \times 10^{20} cm^{-2}$ in NGC 7023 (Buss et al. 1994). The value in M17SW is $2 \times 10^{23} cm^{-2}$ (Stutzki et al. 1988), while in the Orion Bar $N(H_2) \approx 5 \times 10^{22}$ (Hogerheijde et al. 1995). The typical fractional abundance of HCO⁺ in these sources is $\sim 10^{-9}$ to 10^{-8} , while those of HOC⁺ and CO⁺ are generally in the range 10^{-13} to 10^{-12} . CO⁺, however, is a factor of 10–100 more abundant in NGC 7023, Mon R2, and the Orion Bar.

4.2. Abundance Ratios

As described by Ziurys & Apponi (1995), the $[HCO^+]/[HOC^+]$ abundance ratio is best calculated from the ^{18}O isotopomer of HCO⁺, or the ^{13}C species if the former is not available, because the main isotopomer is almost always optically thick. The ratio can be calculated directly from the line temperatures of HC¹⁸O⁺ (or H¹³CO⁺) and HOC⁺ and then

TABLE 4
RELEVANT CHEMICAL RATIOS

Source	$[\text{HCO}^+]/[\text{HOC}^+]^a$	$[\text{HCO}^+]/[\text{CO}^+]^b$	$[\text{CO}^+]/[\text{HOC}^+]^b$
S140	12408	7419	0.6
NGC 2023.....	1913	734	1.3
M17SW	2262 ^c	250 ^{d,e}	9.0
Mon R2.....	460 ^f	148 ^f	3.1
Orion Bar.....	270 ^c	139 ^d	1.9
NGC 7023.....	50–120 ^g	13 ^g	4–12
Model ^h	20–30	...

^a Based on antenna temperature (see Table 1).

^b Based on total column density (see Table 3).

^c From Apponi et al. 1999.

^d Using HCO^+ data from Apponi et al. 1999.

^e CO^+ column density from Störzner et al. 1995.

^f From Rizzo et al. 2003.

^g From Fuente et al. 2003.

^h Sternberg & Dalgarno 1995; based on $N(\text{H}_2) \approx 10^{21} \text{ cm}^{-2}$, $f(\text{HCO}^+) \sim 10^{-12}$ to 10^{-8} .

scaled by the appropriate isotope ratio, as described. The $[\text{HCO}^+]/[\text{HOC}^+]$ ratios thus derived are given in Table 4.

CO^+ is an open-shell molecular ion with a $^2\Sigma$ ground state, while HCO^+ and HOC^+ are closed-shell, $^1\Sigma^+$ species. This difference in energy-level structure means that a direct comparison of antenna temperatures cannot be made to calculate abundance ratios. Furthermore, CO^+ was observed in the $N = 2 \rightarrow 1$ transition and the other molecules in the $J = 1 \rightarrow 0$ line. The abundance ratios involving CO^+ were therefore computed from the total column densities. Because of possible contamination from $^{13}\text{CH}_3\text{OH}$, the $J = 3/2 \rightarrow 1/2$ component was used to estimate the column density, except for the Orion Bar and NGC 7023. The $J = 5/2 \rightarrow 3/2$ component in these cases appeared uncontaminated, so this line was used instead. $[\text{HCO}^+]/[\text{CO}^+]$ and $[\text{CO}^+]/[\text{HOC}^+]$ ratios calculated in this manner are given in Table 4.

5. DISCUSSION

5.1. New $[\text{HCO}^+]/[\text{HOC}^+]$ Ratios: A Strong Geometric Dependence?

The detection of the $J = 1 \rightarrow 0$ transition of HOC^+ in S140 and NGC 2023 is the first time this molecule has been identified in either source. The observations toward S140 yield an $[\text{HCO}^+]/[\text{HOC}^+]$ ratio near 12,408, while the value in NGC 7023 is 1913. These numbers are quite high for what are thought to be PDR sources. For example, this ratio in the Orion Bar is $[\text{HCO}^+]/[\text{HOC}^+] \sim 270$ (Apponi et al. 1999), while that in Mon R2 is 460 (Rizzo et al. 2003). The ratio in S140 is exceptionally large; in fact, it is significantly greater than the normal range of $[\text{HCO}^+]/[\text{HOC}^+] \sim 2000$ –6000 found for molecular clouds (Apponi & Ziurys 1997). As has been discussed, however, S140 is a complicated source. As Figure 1 illustrates, the C I emission traces what apparently are two structures: a ridgelike feature that coincides with the edge of the molecular cloud and appears to be oriented in the direction of HD 211880 and a finger-like extension that reaches into the cloud and encompasses the three infrared sources. As pointed out by Minchin et al. (1993), this secondary source may not be associated with the PDR per se but with the infrared sources and associated outflows. Hence, the HOC^+ measurements were not taken at the optimal PDR position but rather in a region that traces an active molecular cloud core. Furthermore, the 3 mm beam extends well beyond the material traced by C I (see Fig. 1)

and may be encompassing only the tip of the PDR ridge. Thus, the $[\text{HCO}^+]/[\text{HOC}^+]$ ratio is probably not indicative of the PDR gas exclusively but is a combination of the PDR, the surrounding cloud, and its energetic core. Observations made with higher angular resolution are probably needed to better determine the HOC^+ abundance in this source.

The $[\text{HCO}^+]/[\text{HOC}^+]$ ratio of 1913 found in NGC 2023, on the other hand, is on the lower end of the range of values found in molecular clouds by Apponi & Ziurys (1997). However, as shown in Figure 4, the PDR is probably embedded in the front of the molecular cloud, with considerable ambient material behind it. Hence, given the geometry, it is likely that HCO^+ emission is being detected throughout the cloud, not just in the PDR. Interestingly, the $[\text{HCO}^+]/[\text{HOC}^+]$ ratio in NGC 2023 is close to that found in M17SW, where $[\text{HCO}^+]/[\text{HOC}^+] \sim 2260$ (Apponi et al. 1999). Both sources are obvious PDRs; the higher values perhaps indicate that geometrical effects are influencing the observed ratios. Additional observations using higher spatial resolution are certainly needed to verify such a possibility.

5.2. CO^+ and HOC^+ : A Correlation Through C^+

Although both S140 and NGC 2023 have lower densities and UV fields than the Orion Bar, the ionizing conditions are sufficient to produce CO^+ in measurable quantities. The presence of this ion in PDRs of varying conditions confirms that this molecule is an important indicator of these unique chemical environments. CO^+ is in fact predicted to exist only in the outermost layers of PDRs ($A_v < 2$ mag; Sternberg & Dalgarno 1995). This ion may in fact be a better tracer of PDR chemistry than HCO^+ , for example, which models suggest is still being produced at 8 visual magnitudes into the cloud.

Although neither S140 nor NGC 2023 shows a definitive enhancement of HOC^+ relative to HCO^+ , there seems to be a correlation between HOC^+ and CO^+ abundances. As shown in Table 4, as the $[\text{HCO}^+]/[\text{HOC}^+]$ ratios decrease, the $[\text{HCO}^+]/[\text{CO}^+]$ ratios also decrease proportionately. For example, S140 has the largest $[\text{HCO}^+]/[\text{HOC}^+]$ ratio of 12,408 and also the largest $[\text{HCO}^+]/[\text{CO}^+]$ ratio of 7419. The sources with the smallest $[\text{HCO}^+]/[\text{HOC}^+]$ ratios, the Orion Bar and NGC 7023 with 270 and 50–120, respectively, correspondingly exhibit the smallest $[\text{HCO}^+]/[\text{CO}^+]$ values (139 and 13; see Table 4). Furthermore, the $[\text{CO}^+]/[\text{HOC}^+]$ ratios remain relatively constant for all sources. As shown in Table 4, $[\text{CO}^+]/[\text{HOC}^+]$ values lie in the range 1–9. Moreover, they fall in the range 3–9 at all positions measured in the Orion Bar. Therefore, these ratios indicate that the CO^+ and HOC^+ abundances follow similar trends.

This correlation can perhaps be explained because HOC^+ and CO^+ have a common progenitor, C^+ . As shown in the schematic of the $\text{HCO}^+/\text{CO}^+/\text{HOC}^+$ chemical network displayed in Figure 8, CO^+ is destroyed by H_2 . This reaction leads to HOC^+ or HCO^+ in approximately equal amounts (Freeman & McEwan 1987). This synthetic route alone would not explain the observed ratios. However, C^+ leads to CO^+ , HCO^+ , and HOC^+ . The reaction of C^+ and OH or O_2 creates CO^+ , while that with H_2O results in HOC^+ and HCO^+ . In the latter case, the branching ratio heavily favors HOC^+ (84% vs. 16%; Freeman & McEwan 1987). Moreover, the reactions leading to CO^+ and HOC^+ have roughly comparable rates near $k \sim 10^{-9} \text{ cm}^3 \text{ s}^{-1}$, as shown in Table 5. Therefore, it appears that the creation of C^+ in PDRs leads to the selective production of CO^+ and HOC^+ . CO^+ is exclusively formed in PDRs because C^+ is its dominant precursor. HOC^+ is favored in PDRs

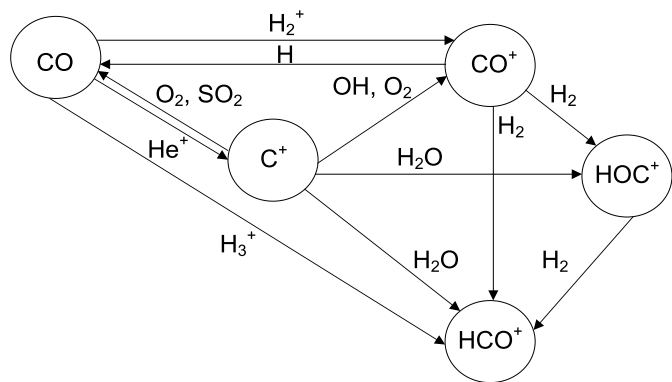


FIG. 8.—Chemical network involving CO^+ , HCO^+ , and HOC^+ . HCO^+ is predominantly produced from the process $\text{CO} + \text{H}_3^+$, while HOC^+ is the favored product from the reaction $\text{C}^+ + \text{H}_2\text{O}$. C^+ is also the major precursor for CO^+ . The abundances of CO^+ and HOC^+ are therefore linked through a common reactant.

because of the $\text{C}^+ + \text{H}_2\text{O}$ reaction. In dense molecular clouds, HOC^+ can be produced with much less yield from $\text{H}_3^+ + \text{CO}$, so it still has some limited abundance in ambient molecular gas.

5.3. Comparison with Theoretical Models

It is difficult to make quantitative comparisons between observational results and theoretical calculations of PDRs, because models are dependent on assumed values of gas density, temperature, and UV flux. In addition, there are no theoretical predictions for HOC^+ abundances. However, some qualitative comparisons can still be made. The most comprehensive model of PDR chemistry is that of Sternberg & Dalgarno (1995). The authors present several chemical networks and predict the abundances of 68 atomic and molecular species using 772 chemical reactions, as well as photodissociation and electron recombination. The assumed UV field is $\sim 10^5 G_0$. Although this model does not include HOC^+ , it considers HCO^+ and CO^+ , using the $[\text{HCO}^+]/[\text{CO}^+]$ ratio as an indicator of different chemical “zones” within the PDR.

As shown in Table 4, the Sternberg & Dalgarno (1995) model predicts $[\text{HCO}^+]/[\text{CO}^+] \sim 20\text{--}30$, for $f(\text{HCO}^+)$ in the range 10^{-12} to 10^{-8} , for $A_v \sim 0.5\text{--}1.5$. As the visual extinction increases to 3, the ratio climbs to almost 7000 and the CO^+ abundance rapidly falls to $f < 10^{-14}$. Hence, the calculated ratio and CO^+ abundance are consistent with the NGC 7023 data, and perhaps with those of the Orion Bar and Mon R2. For the other sources, the observed CO^+ abundance is too high, relative to the $[\text{HCO}^+]/[\text{CO}^+]$ ratio. To accurately model PDR chemistry, HOC^+ abundance probably needs to be evaluated as well, because this species removes HCO^+ .

Any future model will certainly depend on the ionization field and the visual extinction (or hydrogen column density). Qualitatively speaking, the $[\text{HCO}^+]/[\text{HOC}^+]$ ratio does not appear to directly correlate with the FUV flux; NGC 7023 and NGC 2023 have comparable fluxes ($G_0 \sim 2000\text{--}5000$), for example, yet their ratios differ by at least an order of magnitude. Mon R2 has the highest flux of all the sources considered ($G_0 \sim 5 \times 10^5$; Rizzo et al. 2003) but has an $[\text{HCO}^+]/[\text{HOC}^+]$ ratio 4–9 times lower than that of NGC 7023. There appears to be a better correlation with $N(\text{H}_2)$ or A_v . If we compare

TABLE 5
REACTION RATES FOR THE $\text{HCO}^+/\text{HOC}^+/\text{CO}^+$ NETWORK

Reaction	k ($\text{cm}^3 \text{ s}^{-1}$) ^a
$\text{C}^+ + \text{O}_2 \rightarrow \text{CO}^+ + \text{O}$	$(3.8\text{--}7.5) \times 10^{-10}$
$\text{C}^+ + \text{OH} \rightarrow \text{CO}^+ + \text{H}$	$(7.7\text{--}9.9) \times 10^{-10\text{b}}$
$\text{C}^+ + \text{H}_2\text{O} \rightarrow \text{HCO}^+/\text{HOC}^+ + \text{H}$	$2.3 \times 10^{-9\text{c}}$
$\text{C}^+ + \text{O}_2 \rightarrow \text{CO} + \text{O}^+$	$(4.0\text{--}6.2) \times 10^{-10\text{b}}$
$\text{C}^+ + \text{SO}_2 \rightarrow \text{CO} + \text{SO}^+$	$(2.3\text{--}3.5) \times 10^{-9\text{b}}$
$\text{CO}^+ + \text{H}_2 \rightarrow \text{HCO}^+/\text{HOC}^+ + \text{H}$	$(1.8\text{--}2.0) \times 10^{-9}$
$\text{CO}^+ + \text{H} \rightarrow \text{CO} + \text{H}^+$	$(0.9\text{--}7.5) \times 10^{-10}$
$\text{HOC}^+ + \text{H}_2 \rightarrow \text{HCO}^+ + \text{H}_2$	$3.8 \times 10^{-10\text{d}}$
$\text{CO} + \text{He}^+ \rightarrow \text{C}^+ + \text{O} + \text{He}$	1.6×10^{-9}
$\text{CO} + \text{H}_3^+ \rightarrow \text{HCO}^+ + \text{H}_2$	1.7×10^{-9}
$\text{CO} + \text{H}_3^+ \rightarrow \text{HOC}^+ + \text{H}_2$	$(2.7\text{--}9.4) \times 10^{-11}$
$\text{CO} + \text{H}_2^+ \rightarrow \text{CO}^+ + \text{H}_2$	6.4×10^{-10}

^a Rates are from the UMIST Database (Le Teuff et al. 2000) and the OSU New Standard Model, unless otherwise indicated.

^b Temperature-dependent rate is from the OSU New Standard Model; evaluated at 100 K.

^c Rate is from Freeman & McEwan (1987); branching ratio 84% HOC^+ and 16% HCO^+ .

^d Rate is from Smith et al. (2002).

Tables 4 and 5, the sources with the lower H_2 column densities have the smaller $[\text{HCO}^+]/[\text{HOC}^+]$ ratios and vice versa, although there is some degree of scatter. Because the reaction of HOC^+ with H_2 rapidly leads to HCO^+ , increasing the molecular hydrogen column density (or A_v) may increase this ratio. Future modeling should examine this possible observational constraint.

6. CONCLUSIONS

HOC^+ and CO^+ have been identified in two new PDR sources, S140 and NGC 2023, confirming the prevalence of such molecular ions in these regions. Although neither S140 nor NGC 2023 shows significant enhancement of HOC^+ relative to HCO^+ , geometric effects may be masking this ratio, or HCO^+ may be favored in these regions of high H_2 column density. On the other hand, the $[\text{HCO}^+]/[\text{HOC}^+]$ and $[\text{HCO}^+]/[\text{CO}^+]$ ratios appear to be highly correlated. The $[\text{CO}^+]/[\text{HOC}^+]$ ratio in fact is almost constant in value, ranging from 1 to 9 in six PDR sources and across several positions in the Orion Bar. The production of CO^+ and HOC^+ must be connected in PDRs, as line profiles across the Orion Bar indicate. Examination of the ion reaction network suggests that the chemistry of these two species are likely linked via C^+ . This atomic ion rapidly produces both CO^+ and HOC^+ , with a less favorable branching ratio to HCO^+ . Comparison with PDR models suggests that HOC^+ must also be considered for reliability in abundance calculations. These studies also indicate that PDR chemistry cannot fully be understood without considering all important ion species, for which observational data are sorely lacking.

This research is supported by NSF grant AST 02-04913. C. S. wishes to thank NASA for a Graduate Student Researchers Program fellowship, which supported the major portion of this work.

REFERENCES

- Apponi, A. J., Pesch, T. C., & Ziurys, L. M. 1999, *ApJ*, 519, L89
- Apponi, A. J., & Ziurys, L. M. 1997, *ApJ*, 481, 800
- Blair, G. N., Evans, N. J., Vandembout, P. A., & Peters, W. L. 1978, *ApJ*, 219, 896
- Blake, G. A., Sutton, E. C., Masson, C. R., Phillips, T. G., Herbst, E., Plummer, G. M., & Delucia, F. C. 1984, *ApJ*, 286, 586
- Burton, M. G., Hollenbach, D. J., & Tielens, A. G. G. M. 1990, *ApJ*, 365, 620
- Buss, R. H., Allen, M., McCandliss, S., Kruk, J., Liu, J. C., & Brown, T. 1994, *ApJ*, 430, 630
- Chokshi, A., Tielens, A. G. G. M., Werner, M. W., & Castelaz, M. W. 1988, *ApJ*, 334, 803
- DeFrees, D. J., Loew, G. H., & McLean, A. D. 1982, *ApJ*, 257, 376
- DeFrees, D. J., McLean, A. D., & Herbst, E. 1984, *ApJ*, 279, 322
- Freeman, C. G., & McEwan, M. J. 1987, *Int. J. Mass Spectrom. Ion Processes*, 75, 127
- Fuente, A., & Martín-Pintado, J. 1997, *ApJ*, 477, L107
- Fuente, A., Martín-Pintado, J., Neri, R., Rogers, C., & Moriarty-Schieven, G. 1996, *A&A*, 310, 286
- Fuente, A., Rodríguez-Franco, A., García-Burillo, S., Martín-Pintado, J., & Black, J. H. 2003, *A&A*, 406, 899
- Habing, H. J. 1968, *Bull. Astron. Inst. Netherlands*, 19, 421
- Haese, N. N., & Woods, R. C. 1979, *Chem. Phys. Lett.*, 61, 396
- Herbst, E., & Woon, D. E. 1996, *ApJ*, 463, L113
- Herrmann, F., Madden, S. C., Nikola, T., Poglitsch, A., Timmermann, R., Geis, N., Townes, C. H., & Stacey, G. J. 1997, *ApJ*, 481, 343
- Hogerheijde, M. R., Jansen, D. J., & van Dishoeck, E. F. 1995, *A&A*, 294, 792
- Jarroll, M. F., Bowers, M. T., DeFrees, D. J., McLean, A. D., & Herbst, E. 1986, *ApJ*, 303, 392
- Kutner, M. L., & Tucker, K. D. 1975, *ApJ*, 199, 79
- Lada, E. A., Evans, N. J., & Falgarone, E. 1997, *ApJ*, 488, 286
- Le Teuff, Y. H., Millar, T. J., & Markwick, A. J. 2000, *A&AS*, 146, 157
- Lis, D. C., Serabyn, E., Keene, J., Dowell, C. D., Benford, D. J., Phillips, T. G., Hunter, T. R., & Wang, N. 1998, *ApJ*, 509, 299
- Little, L. T., Brown, A. T., MacDonald, G. H., Riley, P. W., & Matheson, D. N. 1980, *MNRAS*, 193, 115
- McNamara, D. H., Madsen, J. B., Barnes, J., & Ericksen, B. F. 2000, *PASP*, 112, 202
- Minchin, N. R., White, G. J., & Padman, R. 1993, *A&A*, 277, 595
- Minchin, N. R., White, G. J., & Ward-Thompson, D. 1995, *A&A*, 301, 894
- Rizzo, J. R., Fuente, A., Rodríguez-Franco, A., & García-Burillo, S. 2003, *ApJ*, 597, L153
- Rosmus, P., & Werner, H. J. 1982, *Mol. Phys.*, 47, 661
- Sastry, K. V. L. N., Helminger, P., Herbst, E., & Delucia, F. C. 1981, *ApJ*, 250, L91
- Smith, M. A., Schlemmer, S., von Richthofen, J., & Gerlich, D. 2002, *ApJ*, 578, L87
- Sternberg, A., & Dalgarno, A. 1995, *ApJS*, 99, 565
- Störzer, H., Stutzki, J., & Sternberg, A. 1995, *A&A*, 296, L9
- Stutzki, J., Stacey, G. J., Genzel, R., Harris, A. I., Jaffe, D. T., & Lugten, J. B. 1988, *ApJ*, 332, 379
- Tauber, J. A., Tielens, A., Meixner, M., & Goldsmith, P. F. 1994, *ApJ*, 422, 136
- Tielens, A. G. G. M., & Hollenbach, D. 1985, *ApJ*, 291, 722
- van der Werf, P. P., Stutzki, J., Sternberg, A., & Krabbe, A. 1996, *A&A*, 313, 633
- Wilner, D. J., & Welch, W. J. 1994, *ApJ*, 427, 898
- Wilson, T. L. 1999, *Rep. Prog. Phys.*, 62, 143
- Wyrowski, F., Walmsley, C. M., Goss, W. M., & Tielens, A. 2000, *ApJ*, 543, 245
- Wyrowski, F., Walmsley, C. M., Natta, A., & Tielens, A. 1997, *A&A*, 324, 1135
- Ziurys, L. M., & Apponi, A. J. 1995, *ApJ*, 455, L73